BNL-222933-2022-TECH

EIC-ADD-TN-028

Thermal analysis of RHIC arc dipole magnet cold mass with EIC beam screen

S. Nayak

April 2022

Electron-Ion Collider

Brookhaven National Laboratory

U.S. Department of Energy

USDOE Office of Science (SC), Nuclear Physics (NP) (SC-26)

Notice: This technical note has been authored by employees of Brookhaven Science Associates, LLC under Contract No.DE-SC0012704 with the U.S. Department of Energy. The publisher by accepting the technical note for publication acknowledges that the United States Government retains a non-exclusive, paid-up, irrevocable, world-wide license to publish or reproduce the published form of this technical note, or allow others to do so, for United States Government purposes.

DISCLAIMER

This report was prepared as an account of work sponsored by an agency of the United States Government. Neither the United States Government nor any agency thereof, nor any of their employees, nor any of their contractors, subcontractors, or their employees, makes any warranty, express or implied, or assumes any legal liability or responsibility for the accuracy, completeness, or any third party's use or the results of such use of any information, apparatus, product, or process disclosed, or represents that its use would not infringe privately owned rights. Reference herein to any specific commercial product, process, or service by trade name, trademark, manufacturer, or otherwise, does not necessarily constitute or imply its endorsement, recommendation, or favoring by the United States Government or any agency thereof or its contractors or subcontractors. The views and opinions of authors expressed herein do not necessarily state or reflect those of the United States Government or any agency thereof.

THERMAL ANALYSIS OF RHIC ARC DIPOLE MAGNET COLD MASS WITH EIC BEAM SCREEN

S. K. Nayak, S. Verdú-Andrés, M. Mapes, J. Tuozzolo, D. Weiss

BNL, Upton, NY 11973, USA

Abstract

The existing RHIC storage rings – including their superconducting magnet arcs – will be used for the hadron storage ring of the Electron-Ion Collider (EIC). The vacuum chamber of these magnets was not designed for the EIC hadron beams, with shorter bunches and of higher average current than the RHIC beams. With the current stainless steel beam pipe, the resistive-wall (RW) heating will exceed the dynamic heat load budget. Limiting the RW heating is important to prevent the superconducting magnets from quenching and to maintain a low screen temperature necessary to impede the rise of RW heating (higher resistance at higher temperature) as well as to achieve desired ultra-high vacuum. In addition, simulations predict the formation of electron cloud which would further contribute to the dynamic heat load and could compromise the quality and stability of the beam. To reduce the resistive-wall heating and suppress electron cloud, a beam screen will be installed in the vacuum chamber of the RHIC SC magnets. The screen will have a high RRR copper layer at its inner face – useful to reduce the resistive-wall impedance thanks to its high conductivity especially at cryogenic temperatures – and will be coated with a thin layer of amorphous carbon, a material with low secondary electron yield to suppress the formation of electron clouds. The baseline solution envisages a screen that will be cooled by thermal contact to the 4.55 K beam pipe. Detailed thermal analysis have been conducted in ANSYS 2020 for an arc dipole cold mass equipped with a beam screen in order to study the feasibility of a passively-cooled screen and guide its design. Temperature-dependent thermal conductivity properties of all materials in the operating (cryogenic) temperature range are considered. Suitable assumptions and simplifications are made to model the magnet coil and calculate its homogenized thermal conductivity. Sensitivity studies with respect to layer thicknesses and area of contact are carried out and results are presented.

INTRODUCTION

An Electron Ion Collider (EIC) will be built at Brookhaven National Laboratory in the coming years. The EIC hadron storage ring will make use of the existing RHIC storage rings including their superconducting magnet arcs [1]. This design choice will spare the project from building new, expensive superconducting magnets. However, the dynamic heat load budget is limited. Excessive RW heating can result in a raise of the beam pipe temperature and in turn degrade the vacuum level or make the superconducting magnets quench. Electron cloud can also generate a significant heat load. An upgrade of the cold sections of the RHIC vacuum chamber is therefore projected to enable reliable operation without compromising the EIC luminosity goal. The upgrade consists in installing a beam screen in the vacuum chamber of the RHIC superconducting magnets [1, 2].

The beam screen must show a small resistive-wall (RW) impedance and prevent the formation of electron clouds. The baseline beam screen design presumes a screen that will be cooled by thermal contact to the 4.55 K beam pipe. Detailed thermal analyses have been carried out to verify the feasibility of this solution and guide its design. The studies focus on a RHIC dipole magnet cold mass equipped with various types of passively cooled beam screens.

THE RHIC ARC DIPOLE COLD MASS

The cross-section of a RHIC arc dipole magnet cold mass [3] is shown in Figure 1. Each dipole magnet is about 10 m long and has 243 m bending radius with 48 mm sagitta. The superconducting coil is assembled from two half-coils (upper and lower half) around the beam pipe with four spacers in between. There are ULTEM6200 horizontal spacers and ULTEM6200 vertical spacers. The 2 mm-thick SS316LN beam tube is wrapped with 76 μm-thick Kapton. Four kelvin helium flows through four channels formed between the spacers, beam tube and coils. The spacers are 2.7 mm thick, 20 mm wide and 76 mm long, spaced 0.3 m away from each other along the beam tube length. The coils are keyed to the ultra-low carbon steel yoke laminations through precision-molded glass-filled phenolic (RX630) insulator spacers. The 4K helium also flows through four round holes opened in the yoke laminations for the passage of the coolant and through the two square slots that host the electrical buses.

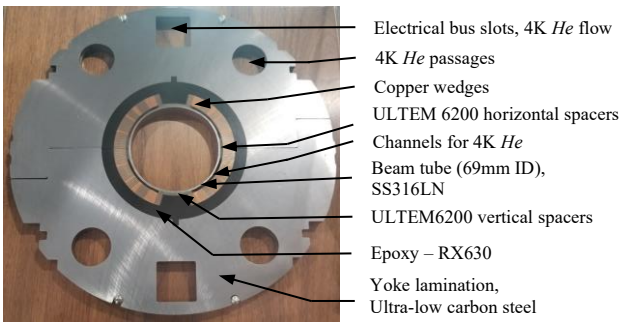

Figure 1: Cross-section of RHIC dipole magnet cold mass

Each half coil (Figure 2) consists of a single layer of 32 turns arranged in four blocks with intervening copper wedges. The superconducting cable is made from 30-strand

wire. Each wire consists of 3510 NbTi filaments arranged in an OFHC copper matrix which is surrounded by an OFHC copper casing. The cable is wrapped with 0.1 mm-thick Kapton [3].

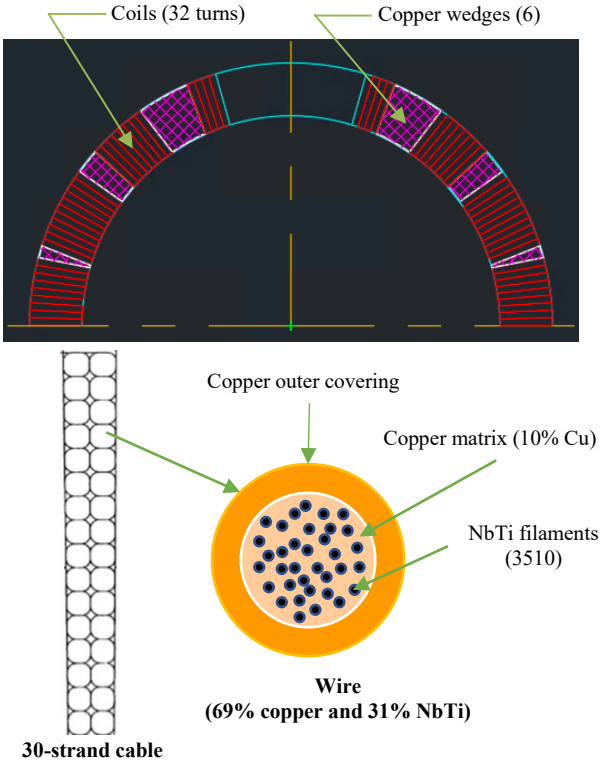

Figure 2: Dipole magnet coil

BEAM SCREEN

With the current stainless-steel RHIC beam pipe, the EIC hadron ring will be vulnerable to electron cloud build-up and high resistive losses from beam-induced currents [2]. The vacuum chamber of the EIC hadron ring will be updated with a beam screen designed to present sufficiently low impedance and low secondary electron-emission yield (SEY). The beam screen is a copper-clad stainless steel shell [4] which internal surface is coated with amorphous carbon. The high RRR copper layer (75 um thick for the beam-induced currents to fully attenuate before reaching the stainless steel) helps to reduce the resistive-wall impedance and conducts the heat well; the stainless steel layer (0.5–1.0 mm thick) is needed for structural purposes; the amorphous carbon film (100 nm thick) helps to mitigate electron cloud thanks to its low secondary electron emission.

The baseline solution employs a beam screen for which the heat will be mainly extracted by conduction through direct contact with the beam pipe [1]. A first design considers a "polygonal" screen (Figure 3) with a circular contour in the horizontal plane that conforms well to the beam tube inner radius to ensure good thermal contact with the beam tube. Its top and bottom sections are ridge-shaped to exert spring action when compressed and undersized to enable the screen to collapse inward and facilitate the insertion through the 10-m long beam tube. Once inserted, wedges are installed to push the ridges towards the centre, which in turn forces the screen to hold in position and to maintain good thermal contact with the beam pipe. A second design consists of a "rolled-up" screen.

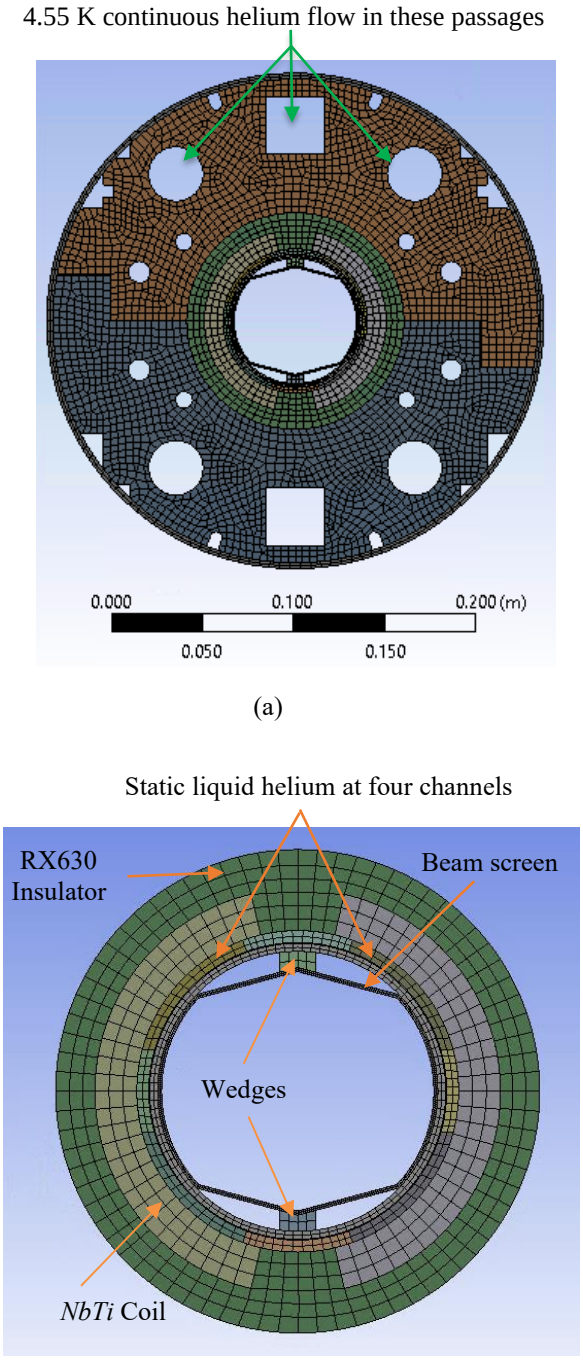

Figure 3: (a) FEA model of transverse cross-section of RHIC arc dipole, (b) Close-up view without yoke and containment vessel

2D THERMAL ANALYSIS

An excessive dynamic heat load can increase the temperature of the vacuum chamber, and in turn, degrade the vacuum level, but can also make the superconducting magnets quench. The main purpose of the thermal analysis is to evaluate the maximum temperature reached at the beam screen and the superconducting magnet coil. The effective surface resistance seen by the beam-induced currents depends on the temperature reached by the beam screen and ultimately determines the resistive-wall heat load to the beam screen. The vacuum conditions in the vacuum chamber will depend on the temperature of the beam screen and the beam pipe. To prevent that the propagation of H_2 from warm sections increases the apparent SEY of the beam screen surfaces seen by the beam, the beam screen needs to be kept at a temperature below 20 K [5]. On the other hand, the temperature at the coil will determine the maximum operational current and thus magnetic field that the magnet can provide before it quenches. Assuming a 5% link margin, the temperature of the coil cannot surpass 5.3 K at the maximum field location during operation with the 275 GeV proton beam, which requires the RHIC arc dipoles to provide a bending magnetic field of 3.8 T [6, 7].

A thermal simulation of the entire RHIC arc dipole magnet would be computationally expensive. Our analysis utilizes the transverse cross section of the magnet, which is basically uniform along the magnet's length except at the two ends. The two-dimensional steady-state thermal analysis has been carried out in ANSYS 2020.

Finite Element Modelling

For our thermal analysis, the nominal thickness of the stainless steel is 1 mm and for copper, 75 µm. The amorphous carbon layer is only about 100 nm and thus not considered in our thermal model. The finite element model of the cross-section of RHIC dipole magnet cold mass with beam screen is shown in Figure 3. Here, the entire coil is modelled as a homogenous material and copper wedges are not part of the model. All the components are meshed using quadrilateral elements for better accuracy. There are very few triangular elements in the yoke as ANSYS could not produce all quadrilateral elements.

Material Properties

Temperature-dependent thermal conductivity (K) values at cryogenic temperatures (Figure 4) [8] are used for all the materials. Table 1 lists the thermal conductivity values at 5 K and 300 K. Since the thermal conductivity of RX630 thermostat plastic and ULTEM6200 at cryogenic temperatures could not be found in literature, we assumed that of G-10 and Kapton, respectively, considering their room temperature values being very close to each other. The thermal conductivity of the specific ultra-low-carbon steel used for the yoke of the RHIC superconducting magnet could not be found either in the operational (cryogenic) temperature range. Typically, the thermal conductivity of low carbon steel is in the range of 25-93 W/m-K at room temperature. Our calculations assume the thermal conductivity of low carbon steel to be three times that of SS304L/SS316L over the whole temperature range.

Table 1: Thermal conductivity of materials

Material	K (W/m-K) at 5 K	K (W/m-K) at 300 K
SS304L/316LN	0.366	15.3
Low carbon steel	1.1	45.9
OFHC Copper, RRR=50	391.9	392.4
OFHC Copper, RRR=100	783.2	396.3
Coil	0.576	9.4
Kapton	0.011	0.19
G-10	0.084	0.6
Helium	0.021 (4 bar pressure)	-
Nb-Ti	0.2-0.4	-

As depicted in Figure 2, the coil is not a homogenous material. The following assumptions were made to simplify the model and reduce the simulation computing time. Since Nb-Ti is a very poor thermal conductor in comparison to copper, we assumed that the heat gets conducted through the copper outer-casing of the wire which constitutes 59% of wire material [3]. The effective thermal conductivity of the cable along the radial direction, given that the cable is wrapped with 0.1 mm-thick Kapton insulation, is calculated as shown in Figure 5. The thermal conductivity of the cable is applied to the coil as a homogenized property. No separate thermal conductivity along the circumferential direction is considered here. The copper wedges are not included in our model.

Thermal Contacts

Perfect thermal contacts are considered between all insulators, and between insulators and metals. A thermal contact conductance (TCC) of 5 W/m^2-K is applied between all surfaces of the beam screen and beam pipe in contact.

The TCC depends upon the type of materials in contact, surface finish of the contacting faces, contact pressure, temperature, and vacuum level. TCC between two stainless steel (SS) surfaces in air at room temperature and 1-10 atm contact pressure is 2000-3700 W/m^2-K [9], dropping to 400-1667 W/m^2-K in vacuum [9]. Limited TCC data are available for contact pressures below 1 atm at cryogenic temperatures as is expected in our design. The TCC between SS at 1/8 atm contact pressure, in vacuum and at about 65 K is about 100 W/m^2-K [10]. As a conservative approach, a low TCC (5 W/m^2-K) is considered in this study.

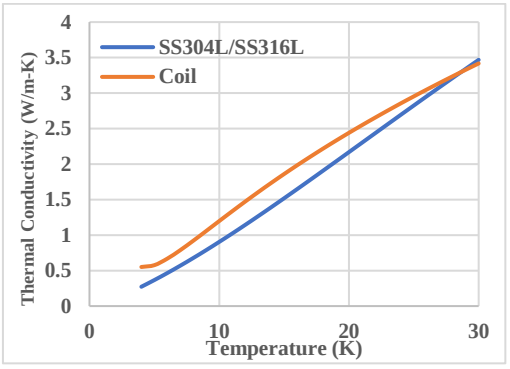

(a)

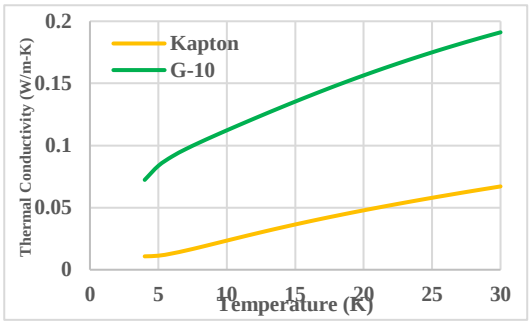

(b)

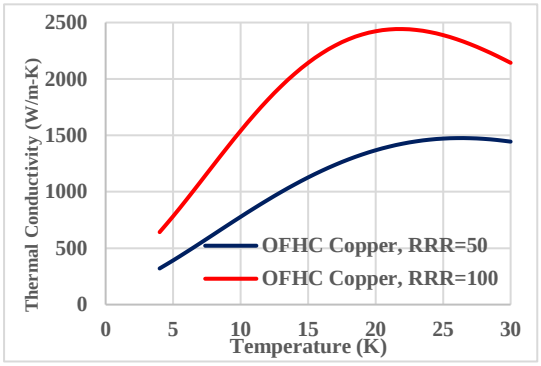

(c)

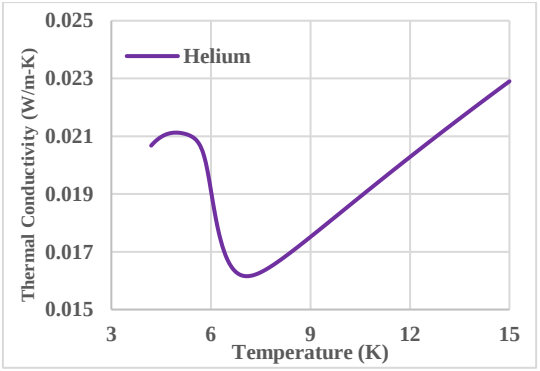

(d)

Figure 4: Thermal conductivity in the cryogenic temperature range for (a) SS304L/SS316L and coil, (b) Kapton and G10, (c) OFHC Copper and (d) Helium

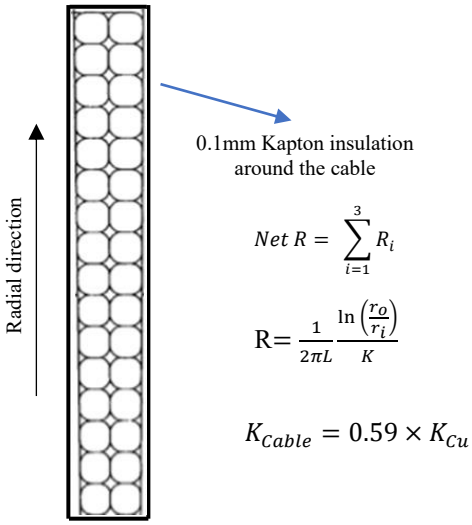

Figure 5: Thermal conductivity of coil. R – thermal resistivity, r_0 – outer radius, r_i – inner radius and L – length

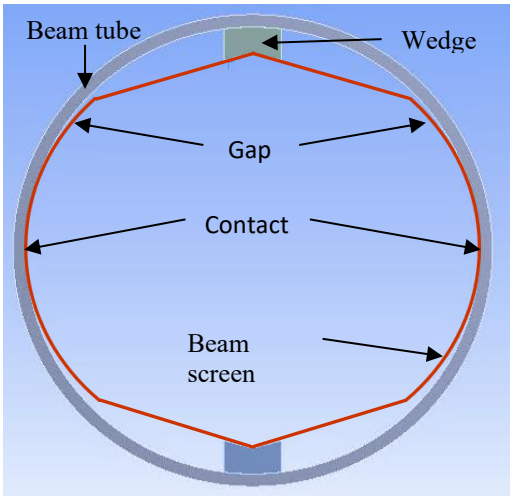

(a)

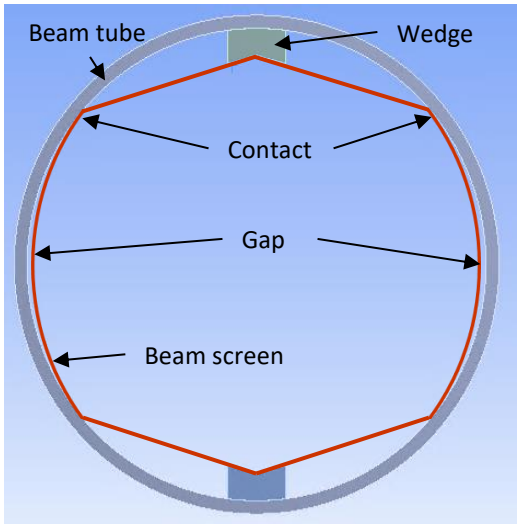

(b)

Figure 6: Two types of contact scenarios: (a) contact starts at mid-plane, or (b) from four corner areas.

Though the aim is to maximize the area of contact between the beam screen and the beam tube, gaps will unavoidably appear in some part of intended contact area due to geometric imperfections of beam tube and the screen. Two scenarios are considered (Figure 6). Contact areas and gaps are assumed symmetric in both cases. Analyses are carried out at different percentage of intended contact area.

Boundary Condition

Supercritical helium flows at 4 bar pressure through the two square electrical bus slots and four round holes in the yoke, where a temperature boundary condition of 4.55 K is applied. The temperature rises of the coolant as it extracts heat on its way from one end of the magnet to the other is expected not to exceed 150 mK. The four helium flow channels around the beam pipe have 2.7 mm radial spacing with magnet coils. The straight dipole assembly was pressed into a curved shape during fabrication, and in consequence, the dimensions of the annular channel around the beam pipe are uncertain. The spacers between beam pipe and coils are found every 0.3 meters over the full length of the magnet. We assume the worst-case scenario, that is, the He flow through the annular channel is minimal or even null, hence no temperature boundary conditions are applied here. The coolant is modelled to transfer the heat through conduction.

Dynamic Heat Load

Assuming that the electron cloud build-up is suppressed by the low SEY of the amorphous carbon film, the main source of dynamic heat load is the RW heating from the beam-induced currents. The expected power dissipation for the most demanding operating scenario is 0.37 W/m when the screen is at 10 K and copper has a RRR > 100. This estimate includes the RW heating from the 290 6 cm-long bunches of the 275 GeV EIC proton beams circulating with a 20 mm offset, the impact of magnetoresistance, and screen geometry. The contribution from the thin amorphous carbon layer is negligible [14].

Although the electrical resistivity of copper, and in turn the RW heating, increase with temperature [11, 12, 13, 14], the variation is small when the temperature is lower than 30 K and thus our thermal simulations assume constant dynamic heat load independent of temperature. For a centred beam, a uniform heat load is applied across the screen perimeter, although the straight sections will get more heat due to its proximity to the beam. For an offset beam, the total power dissipation increases by a factor F (see Eq. 1 [15, 16]), with the power distribution for a round beam screen following Eq. 2 [17]. For a polygonal screen, the power distribution is calculated with CST Microwave Studio (Fig. 7, 8). The resulting temperature distribution is presented in Fig. 10 for a total RW heating of 1.1 W/m.

$$F = \left[\frac{b^2 + x^2}{b^2 - x^2}\right] = 2.1 \text{ for } x = 20\,mm \qquad (1)$$

$$\frac{dF(\theta)}{d\theta} = \left[\frac{b^2 - x^2}{b^2 + x^2 - 2bx\cos\theta}\right]^2 \qquad (2)$$

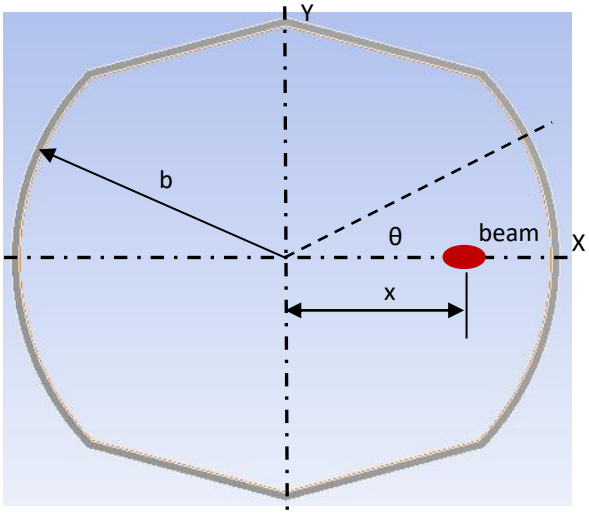

Figure 7: Offset beam and beam screen details for calculating heat load distribution.

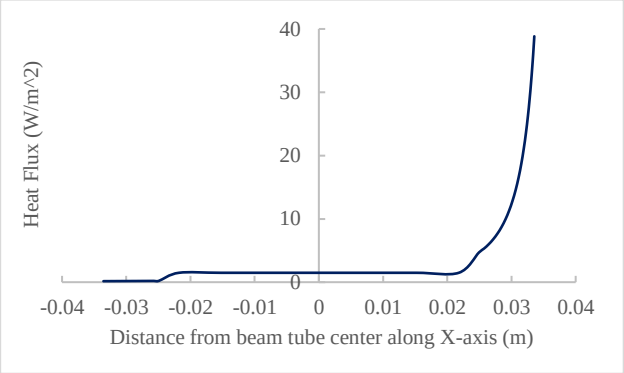

(b)

Figure 8: Heat load profile on beam screen for 20 mm offset beam and 1.1 W/m power dissipation where b is the beam screen radius (33.55 mm) and x is the beam offset. Since most of the power is dissipated in the skin of the screen's surface, the heat load is applied in the form of heat flux to the copper surface.

Results

The temperature distribution reached in the cross section of the cold mass for a beam travelling 20 mm off-centre which delivers a total of 1.1 W/m is shown in Fig. 9. A 1.1 W/m heat load is particularly conservative considering that the RW heat will be lower than 0.5 W/m if the screen is kept below 30 K and the copper has a RRR > 25 [14]. Results for a total heat load of 0.5 W/m delivered by a 20 mm offset beam are presented in Table 2. Moreover, the highest temperature point does not coincide with the location of highest magnetic field, thus further enlarging the safety margin [12].

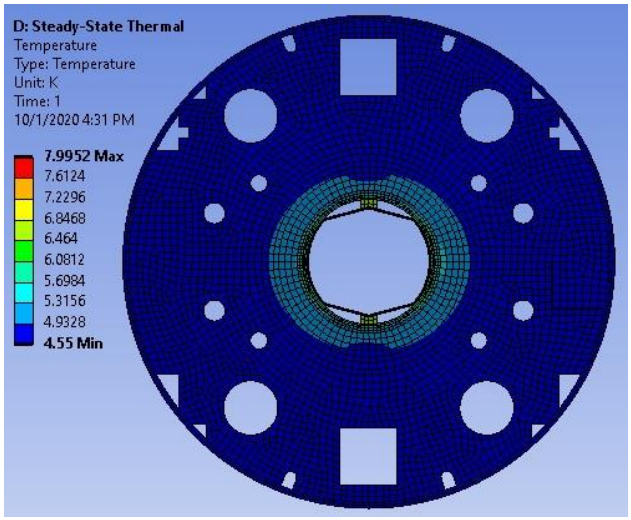

(a)

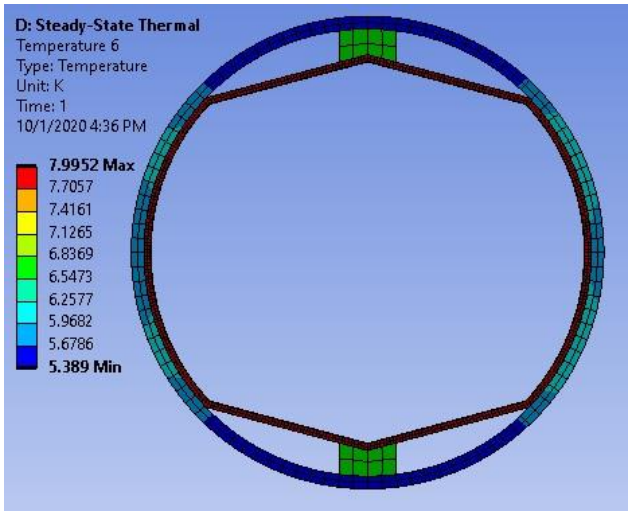

(b)

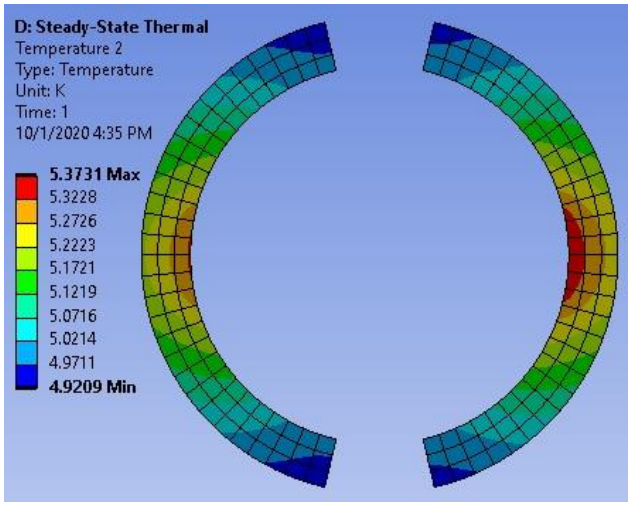

(c)

Figure 9: Temperature plots for 1.1 W/m, 20 mm off-centered beam (a) Entire cold mass, (b) Beam tube with beam screen and (c) Superconducting coil

Table 2 summarizes the results about the effect of the copper thickness. Copper and stainless steel will be joined by diffusion bonding. Some analyses are carried out assuming a conservative 25 µm thick bonding interface for which stainless steel properties are applied (low thermal conductivity). A 75 µm thick copper layer is sufficient to guarantee good heat distribution, even when considering a 25 µm bonding interface with low thermal conductivity. No significant changes in temperature are found when reducing the stainless steel thickness or adding outer copper layer, as illustrated in Table 3.

Table 2: Effect of Cu thickness on temperature

Cu thickness (µm)	**Max. screen temperature (K)**	**Max. coil temperature (K)**
Centered beam, total power = 0.5 W/m		
75	6.1	4.9
100	6.1	4.9
125	6.1	4.9
20 mm offset beam, total power = 1.1 W/m		
75	8.0	5.4
100	8.0	5.4
125	8.0	5.4
20 mm offset beam, total power = 0.5 W/m		
75	6.157	4.937
100	6.144	4.934
1000	6.098	4.925
10000	6.094	4.924
20 mm offset beam, total power = 0.5 W/m with 25 µm thick interface		
50	6.188	4.942
25	6.274	4.959

Table 3: Effect of stainless steel thickness reduction and the addition of an outer copper layer on temperature

Beam screen	**Max. screen temperature (K)**	**Max. coil temperature (K)**
1mm SS with 75µm inside Cu	7.9953	5.3731
0.5mm SS with 75µm inside Cu	7.9951	5.3744
0.5mm SS with both inside and outside Cu, 75µm	7.9398	5.3631

Table 4 presents the maximum temperatures reached at the beam screen and coil for different percentage of contact area between the curved sides of the beam screen and the beam pipe illustrated in Figure 6. A fixed TCC of 5 W/m2-K is assumed for all the contact areas. While a reduction of the contact area could translate into an increase of the contact pressure at those points where contact exists, hence leading to higher TCC values that could counteract the impact of having a reduced contact area, reproducibility could be compromised. The large dependence of the screen temperature on the contact area thus highlights how critical it is to develop an installation mechanism that ensures sufficient contact area for the passively cooled screen to work.

Table 4: Effect of area of contact on temperature.
Contact scenario - Figure 6(a):
20 mm offset beam, total power = 1.1 W/m

% Area of curved-side contact	Max. screen temperature (K)	Max. coil temperature (K)
100	7.9953	5.3731
76	8.6152	5.4192
57	9.3926	5.4508
38	10.772	5.4663
19	14.013	5.4256
1	29.802	5.3335

Contact scenario - Figure 6(b):
20 mm offset beam, total power = 1.1 W/m

% Area of curved-side contact	Max. screen temperature (K)	Max. coil temperature (K)
100	7.9953	5.3731
81	8.4608	5.3127
62	9.1974	5.2497
43	10.397	5.188
24	12.865	5.1635
1	29.861	5.3513

3D THERMAL ANALYSIS

A simple rolled-up screen is considered as an alternative to the screen compressed against the beam pipe by wedges. For a 1 inch-long screen inserted into a straight beam pipe, contact simulations find a minimum guaranteed contact of 13% at three areas of the rolled-up scree circumference, as shown in the Figure 11. The thermal contact conductance in these contact areas must be at least 5 W/m^2-K to limit the temperature rise in the screen, as shown in Figure 12. The temperature increase at the coil is negligible and remains below 5.0 K independently of the TCC value.

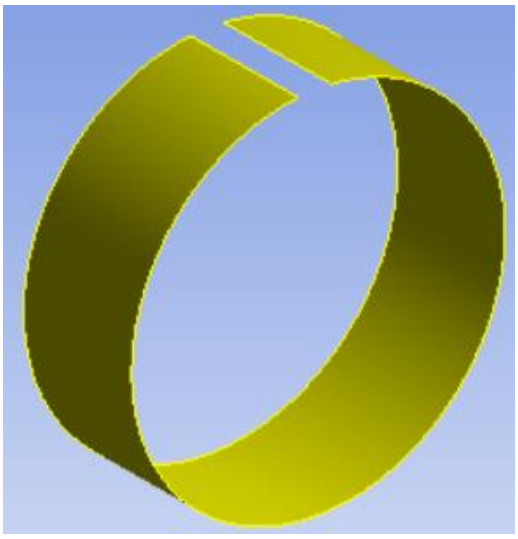

(a)

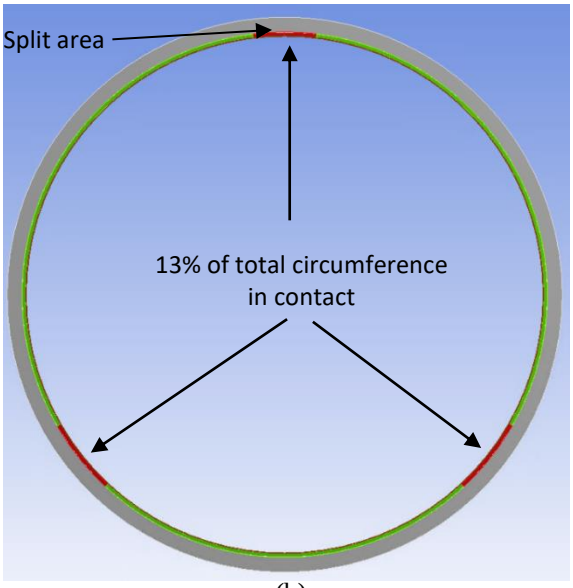

(b)

Figure 11: (a) An oversized simple rolled up beam screen (b) Rolled up beam screen pressed fit inside the beam tube showing area in contact

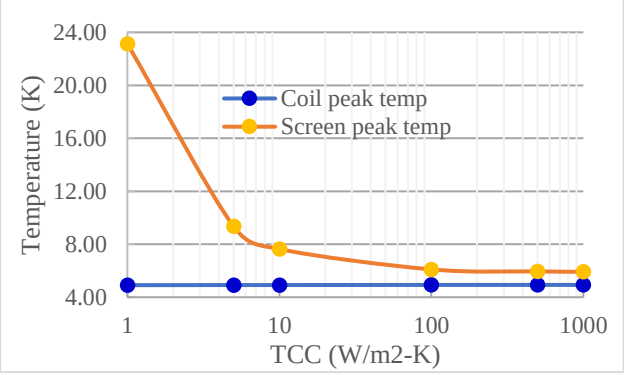

Figure 12: Temperature vs TCC for 0.5 W/m deposited by 20 mm off-centered beam on rolled up screen with 13% area of contact. Coil temperature stays below 5 K.

The beam pipe of a RHIC arc dipole is about 10 meters long and has a sagitta of about 48.5 mm. A 3-D contact simulation for a 10 meter-long rolled-up screen inserted into such beam pipe further revealed that the contact shown in Figure 11 is not continuous along the length of the beam screen. To determine which would be the maximum non-contact length for the screen to still guarantee performance, 3D simulations were performed for a screen of variable length that only established contact at 13% of the circumferential area – as shown in Figure 11 (b) – over a 35 mm long strip at both ends of the screen – as illustrated in Figure 13. The maximum temperature at the screen and the coil goes up (Figure 14) as the non-contact length increases. A 200 mm non-contact length would be the maximum allowed to keep the coil temperature within the allowable limit to avoid quench. Such short length shows the need to develop a mechanism that guarantees contact between the screen and the pipe. Despite the absence of contact, the temperature gradient along the screen is very small (< 3.5 K) thanks to highly conductive copper layer.

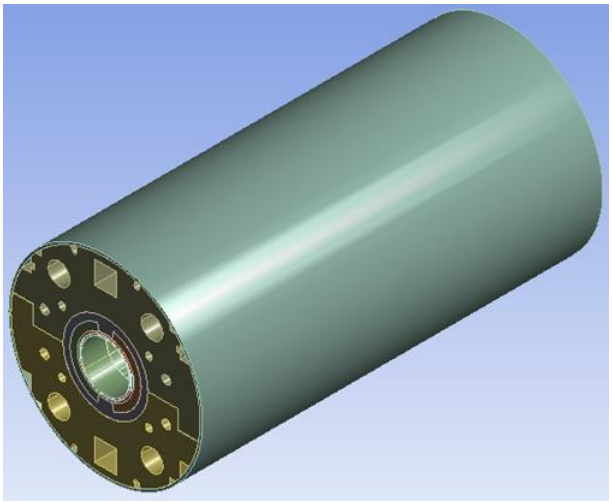

(a)

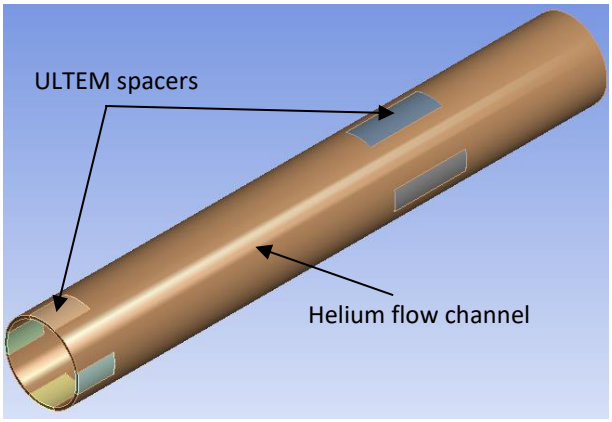

(b)

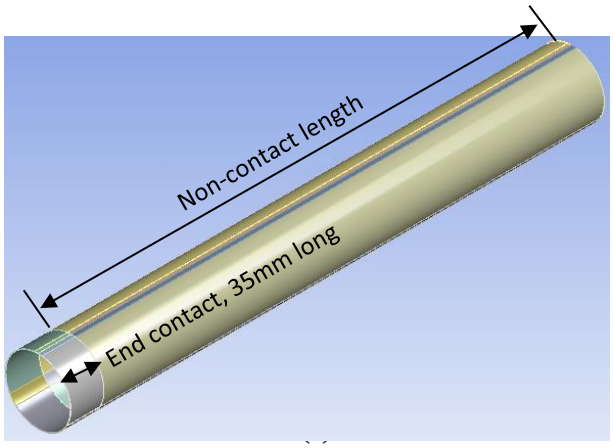

Figure 13: Half-symmetric along the length 3D model (a) Cold mass model (b) ULTEM spacer and He channel (c) Beam screen showing contact and non-contact length

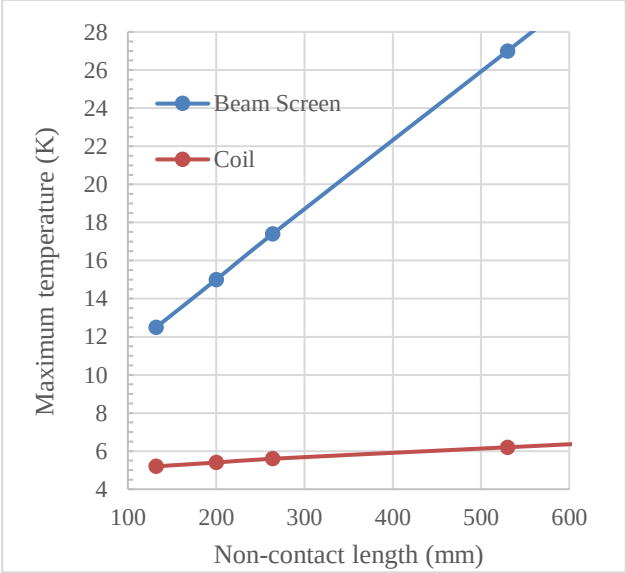

Figure 14: Temperature vs non-contact length for 0.5 W/m deposited by 20 mm off-centered beam on rolled up screen with TCC = 5 W/m2-K.

The results presented above are based upon the assumption that the thermal conductivity of the RX630 insulator and ULTEM6200 spacers are equal to the thermal conductivity of G-10 and Kapton, respectively. Once thermal conductivity data of RX630 and ULTEM 6200 at cryogenic temperatures became available [18], thermal simulations were repeated for two specific cases using these measured values, leading to no significant changes (Table 5).

Table 5: Impact of thermal conductivity for RX-630 and ULTEM 6200 on screen and coil temperatures (TCC = 5 W/m^2-K, 0.5 W/m heat load-20 mm offset beam)

Thermal conductivity of RX630 and ULTEM 6200 assumed to be G-10 and Kapton respectively		
	Polygonal screen with wedges	Rolled-up screen with 13% area of contact
Max. screen temperature (K)	6.37	9.38
Max. coil temperature (K)	4.88	4.92
Measured thermal conductivity of RX630 and ULTEM 6200 [18]		
	Polygonal screen with wedges	Rolled-up screen with 13% area of contact
Max. screen temperature (K)	6.31	9.35
Max. coil temperature (K)	4.98	4.99

DISCUSSION AND CONCLUSIONS

The cold sections of the RHIC vacuum chamber will be updated with a beam screen that presents sufficiently low impedance and secondary electron yield to guarantee operation with the EIC beams. The baseline design considers the implementation of a screen passively cooled by contact to the 4.55 K RHIC beam pipe. The expected RW heat deposition to a screen with copper RRR > 25 at temperatures below 30 K from the worst-case scenario beam (275 GeV proton beam with 290 bunches traveling with 20 mm offset) is 0.5 W/m. Two-dimensional steady-state simulations of the RHIC dipole magnet cold mass with a copper-clad stainless steel screen found that a total 0.5 W/m heat load would lead to a maximum temperature of 6.3 K at the screen and 5.0 K at the coil (Table 6), low enough to guarantee operations.

The maximum temperature in the coil appears in the horizontal plane, at the point which is closest to the beam. This can be explained by the higher heat flow in the horizontal direction due to better conducting path: the thermal conductivity of the ULTEM6200 spacers installed in the horizontal plane, between the beam pipe and the coil, is two to three times that of liquid helium. A copper layer of 75 um is sufficient to guarantee a good heat distribution, even when considering a 25 um thick bonding layer (Table 2). Even though the heat flux is significantly high on the beam screen near the offset beam (Fig. 7, 8), the temperature gradient across the screen profile is only 0.22 K thanks to the copper being a good heat conductor. The temperature gradient in the coil is low for the same reason. Reducing the thickness of the stainless-steel layer from 1 mm to 0.5 mm had no impact on the temperature since copper dominates the heat conduction (Table 3). Adding a copper layer at the outer face of the screen barely reduced the temperature of the screen. The main purpose of this copper outer layer would be to improve the TCC with the beam pipe, since copper has lower stiffness and hardness in comparison to stainless steel and prevent cold welding of the screen and the stainless steel pipe during insertion.

The screen temperature increases steadily by decreasing the contact area (Table 4). However, the coil temperature will remain relatively the same. For a given heat load, the steady-state coil temperature is not very sensitive to TCC, area of contact and thermal conductivity. For a rolled-up beam screen, a 13% contact area is sufficient to keep the temperature of screen and coil at bay with a TCC of 5 W/m2-K. A 3D thermal simulation with varying non-contact length revealed that a maximum of 200 mm non-contact length could be allowed to keep the coil temperature below the quench temperature.

In this study, a conservative TCC (5 W/m^2-K) is used. Given the critical impact that the TCC has on the temperature profile of the cold mass, further studies and experiments are planned to measure the TCC between copper and stainless steel in vacuum at cryogenic temperatures and its dependence on contact pressure. The contact area between screen and beam tube could be somewhat random and intermittent with non-contact areas along the length due to fabrication tolerances. A thermal test of a full beam screen inside a beam tube is planned to measure the temperature profile in the beam screen and assess if its design guarantees the performance requirements.

ACKNOWLEDGEMENT

The authors are grateful to M. D. Anerella, M. M. Blaskiewicz, J. M. Brennan, R. Gupta, G. McIntyre, S. Peggs, S. Sharma and R. Than for useful discussions about the beam screen design, simulation results and different aspects of RHIC dipole magnet design, construction, and operational parameters.

REFERENCES

[1] F. Willeke et al., “Electron ion collider conceptual design report”. EIC Technical Report, BNL, Upton, NY (2021).

[2] S. Verdu-Andres et al., “A beam screen to prepare the RHIC vacuum chamber for EIC hadron beams: conceptual design and requirements”, Proc. of IPAC’21, Campinas, Brazil, May 2021, paper TUPAB260.

[3] RHIC Config Manual: https://www.bnl.gov/cad/accelerator/docs/pdf/RHICConfManual.pdf

[4] G. P. Cruikshank et al., “Mechanical Design Aspects of the LHC Beam Screen”, LHC Project Report 128, CERN, Geneva (1997).

[5] D. Weiss, M. Mapes, J. E. Tuozzolo, and S. Verdú-Andrés, “EIC Hadron Storage Ring Beamline Vacuum Studies”,

Proc. of IPAC'21, Campinas, Brazil, May 2021, paper WEPAB189.

[6] R. Gupta, priv. communication.

[7] S. Peggs, priv. communication.

[8] "Properties of solid materials from cryogenic to room temperatures", NIST: https://trc.nist.gov/cryogenics/materials/materialproperties.htm

[9] "Thermal Contact Resistance", SolidWorks: http://help.solidworks.com/2012/English/SolidWorks/cworks/Thermal_Contact_Resistance.htm

[10] S. S. Kumar, and K. Ramamurthi, "Thermal contact conductance of pressed contacts at low temperatures", Cryogenics 44 (2004) 727–734.

[11] F. Bloch, "Zum elektrischen Widerstandsgesetz bei tiefen Temperaturen" [Electrical resistance law for low temperatures]. Zeitschrift fur Physik (in German) 59 (3-4) 1930.

[12] E. Gruneisen, "Die Abhangigkeit des elektrische Widerstandes reiner Metalle von der Temperatur" [The temperature dependence of electrical resistance in pure metals]. Annalen der Physik (in German), 408 (5) 1933.

[13] M. Deutsch, "An accurate analytic representation for the Bloch-Gruneisen integral", Journal of Physics A: Mathe matical and General, 20 (13) 1987.

[14] S. Verdu-Andres, "Impedance in the HSR screen". Talk at the EIC Review on Collective Effects, BNL, Upton, NY (2021).

[15] A. Piwinski, "Wakefields and ohmic losses in round vac uum chambers", DESY HERA 92-11, DESY, Hamburg (1992).

[16] A. W. Chao, "Physics of collective beam instabilities in high-energy accelerators". John Wiley& Sons,1993.

[17] R. T. Avery, A. Faltens, and E. C. Hartwig, "Non-Intercepting Monitor of Beam Current and Position", Proc. of the 4th Particle Accelerator Conference, Chicago, IL (IEEE, Piscataway, NJ, 1971), pp. 920-922.

[18] J. Lu et al., "Thermal conductivity of RHIC superconducting magnet insulation materials at low temperatures", Technical Note BNL-222821-2022-TECH, Brookhaven National Laboratory, Upton, NY (2022).

SUPPLEMENTAL MATERIAL

Models used for contact pressure calculation in ANSYS

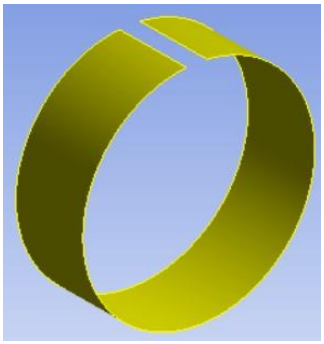

25 mm long beam screen is pressed into straight beam tube.

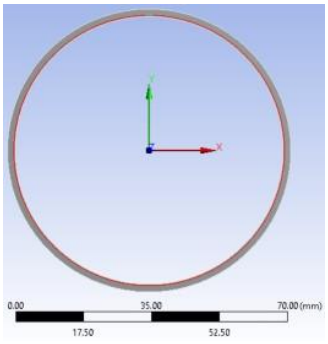

Case1: Free form beam screen dia = 69.75 mm

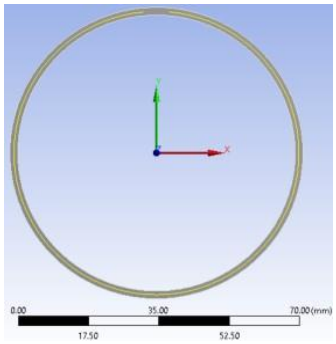

Case2: Free form beam screen dia = 71 mm

- Larger dia rolled beam screenis squeezed intothe beam tube and resulted contact pressure is calculated.
- Initially 25mm long straight beam tubes is considered.
- Beam screen dia 69.75 mm and 71 mm, thickness 0.5 mm and 1 mm are considered.

Results: Contact pressure calculation in ANSYS (screen thickness = 0.5 mm)

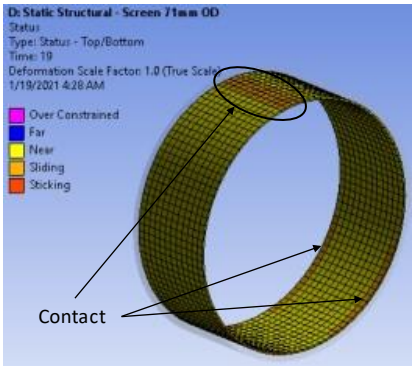

Contact status

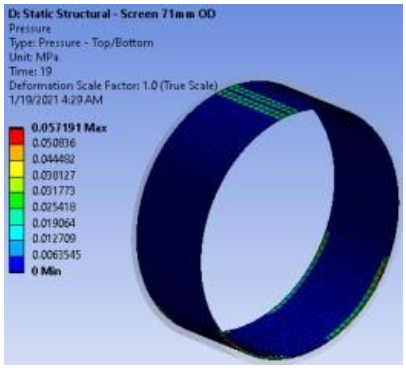

Contact pressure

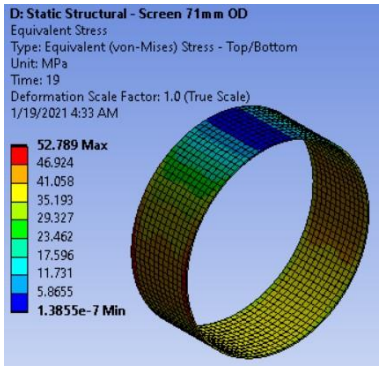

Stress

Results from Preliminary Analysis

Beam Screen

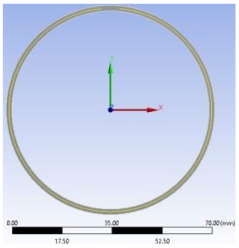

Beam Screen and Beam tube

Beam tube ID = 69 mm

Free form OD of beam screen = 71mm

Parameters	**Beam screen details**			
	t = 0.5mm d_{free} = 69.75 mm	t = 1mm d_{free} = 69.75 mm	t = 0.5mm d_{free} = 71 mm	t = 1 mm d_{free} = 71 mm
Average Contact Pressure, *Kpa (atm)*	0.63 (1/161)	4.6 (1/22)	1.9 (1/53)	14.6 (1/7)
Max stress in beam screen (*MPa*)	18	37	53	107

Results: Contact status in inserting 10m long beam screen in to beam tube

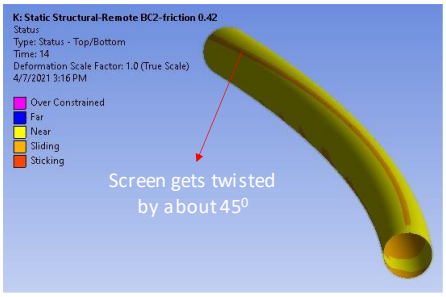

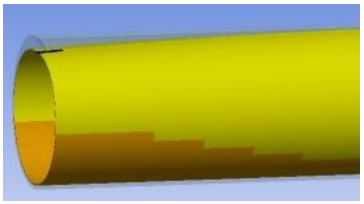

Ignore the excessive deformation at the entrance
Another load step is required to release the RD BC from that edge and produce good result

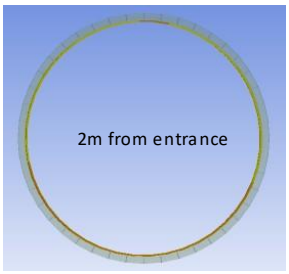

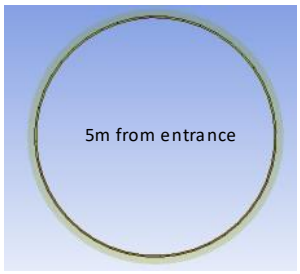

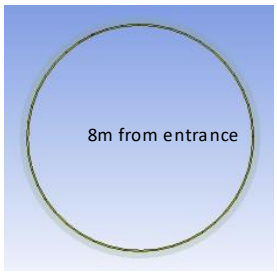

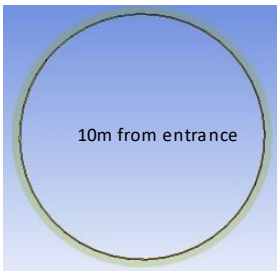

No visible gap is noticed along the length

Results: Area of contact

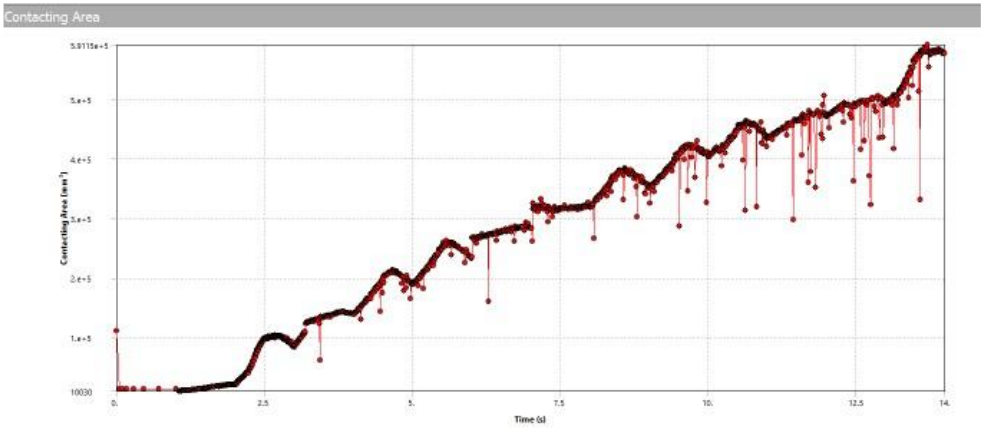

- Area of contact = 27.27%
- 13% area of contact with TCC = 5 W/m^2-K has produced acceptable result.

Results: Contact pressure

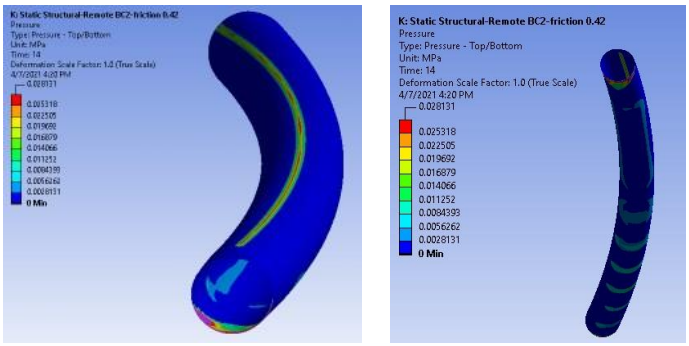

- Average contact pressure = 2.25 KPa (1/45 atm)
- Average contact pressure obtained from straight tube and screen = 1KPa
- Low effect of bending on contact pressure.

Results: Insertion force

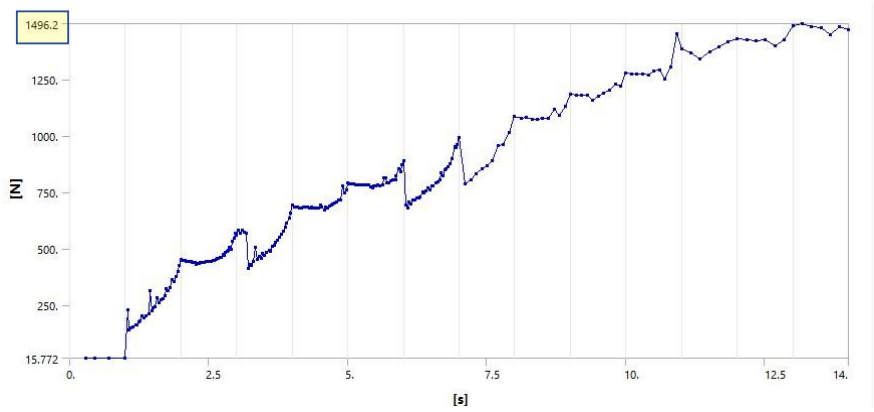

- Insertion force from hand calculation for straight tube and 2.25 KPa contact pressure = **2048 N**
- Average pulling force for 8.75" long screen = 11 lb (49 N), if extrapolated to 10m length in a straight beam tube, pulling force = **2205 N**

Summary

- An uniform good contact is maintained at the seam and large area at the bottom side of screen has good contact, though not uniform along the length.
- Average contact area is 27% which is expected to keep the peak temperature values within limit.
- Screen gets twisted by about 45°.
- Average contact pressure is 2.25 KPa.
- Insertion force is 1500 N which appears to be low in comparison to test results and hand calculation.

3D Thermal simulation (0.5 W/m offset beam, 13% area contact at ends, 1128mm long)

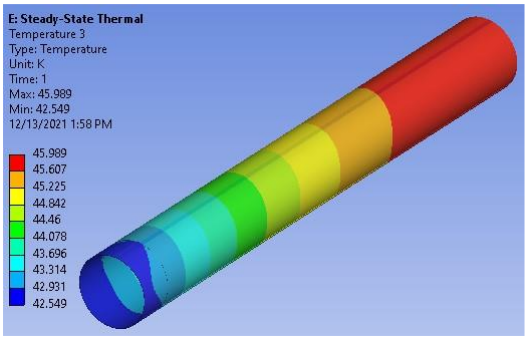

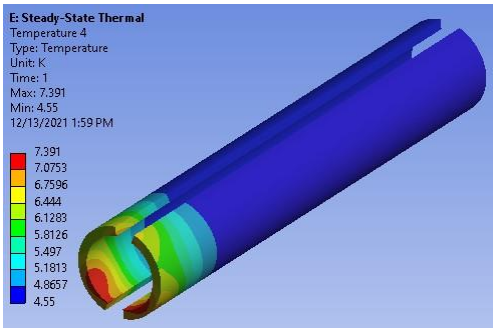

Results

Non-contact length = 200mm

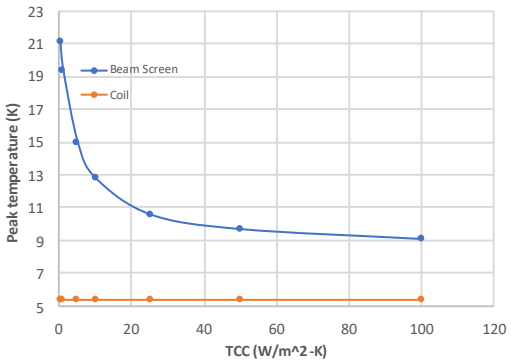

End contact length=35mm, 13% area, non-contact length = 200mm		
TCC (W/m^2-K)	**Peak screen temp (K)**	**Peak coil temp (K)**
0.2	21.1	5.4
1	19.4	5.4
5	**15**	**5.4**
10	12.8	5.4
25	10.6	5.4
50	9.7	5.4
100	9.1	5.4

Result Comparison: 0.5 w/m offset beam load

Thermal contact, TCC = 5 W/m^2-K
0.5 W/m heat load-offset beam

Cases	*Beam Screen Peak Temp (^{0}K)	**Beam Screen Peak Temp (^{0}K)	*Coil peak Temp (^{0}K)	**Coil peak Temp (^{0}K)
Polygonal	6.37	6.31	4.88	4.98
Rolled beam screen with 13% area of contact	9.38	9.35	4.92	4.99

*K of insulator RX630 assumed to be of G-10 = 0.084 W/m-K @ 5K, K of spacer ULTEM6200 assumed to be of Kapton= 0.011 W/m-K @ 5K
** K of insulator RX630 = 0.0608 W/m-K @ 5K, K of spacer ULTEM6200 = 0.03 W/m-K @ 5K from FSU lab testing.